

Magnetic Studies of Some Orthoferrites

D. TREVES*

Bell Telephone Laboratories, Murray Hill, New Jersey

(Received October 30, 1961)

This paper describes a method to distinguish between two mechanisms that may cause weak ferromagnetism in the orthoferrites, i.e., antisymmetric exchange and single-ion magnetocrystalline anisotropy. The free energy of a magnetic crystal is expressed as a series in the applied field. The condition of invariance of the energy with respect to the magnetic point group of the crystal, determines the coefficients of the energy series that are needed to describe the magnetic properties of the crystal. Magnetization and static torque measurements make possible the evaluation of these coefficients, including those of the terms cubic in the applied field. These coefficients are also calculated for the antisymmetric exchange and the single-ion magnetocrystalline anisotropy interactions. The comparison between the measured and calculated coefficients shows that in the orthoferrites the antisymmetric exchange mechanism is predominant. The method described is quite general and should be applicable to a variety of other materials.

1. INTRODUCTION

It has been found by various investigators¹ that many materials with the composition $M\text{FeO}_3$, where M stands for yttrium or a rare earth, exhibit weak ferromagnetism. The structure of these orthoferrites was solved by Geller.² These compounds belong to the space group $D_{2h}^{16}-Pbnm$ with four distorted perovskite units in the true crystallographic unit cell.

In all the compounds of this group studied by neutron diffraction,³ it was found that at room temperature the iron lattice is approximately antiferromagnetic, each ion having six antiferromagnetic nearest neighbors.

The repeatability of the results of measurements of the weak ferromagnetism by various groups,¹ suggests that it is an intrinsic property of these compounds. Dzyaloshinsky⁴ has shown that weak ferromagnetism, caused by canting of the spins in an essentially antiferromagnetic crystal, is in some cases compatible with the symmetry of the antiferromagnetic state.

Moriya⁵ studied the physical interactions that could be responsible for the canting of the spins. He found two such interactions:

1. Single-ion magnetocrystalline anisotropy. In this mechanism the magnetocrystalline easy direction of magnetization is different for the nonequivalent magnetic ions, energetically favoring spin canting.

2. Antisymmetric exchange interaction. This interaction has the form $\mathbf{D}_{ij} \cdot \mathbf{S}_i \times \mathbf{S}_j$, which tends to align the two interacting spins \mathbf{S}_i and \mathbf{S}_j perpendicular to each other, and perpendicular to the constant vector \mathbf{D}_{ij} .

Different magnetic properties are associated with these two mechanisms, so that by performing magnetic measurements one may hope to find which of the two interactions is responsible for weak ferromagnetism in a particular case. With this purpose in mind, static torque measurements were carried out on single crystals of Y, La, and Lu orthoferrites. These nonmagnetic ions were chosen so as to avoid possible contributions to the torque of the anisotropic paramagnetic susceptibility of the rare earth ions.

The torque as a function of the applied field in the various crystallographic planes is calculated for each mechanism of interaction. Comparison of these calculated values with experimental results indicates that in these materials antisymmetric exchange is the predominant interaction responsible for weak ferromagnetism.

2. SPIN STRUCTURES OF THE ORTHOFERRITES

The point group D_{2h} of these materials has the symmetry elements $G = E, C_{2x}, C_{2y}, C_{2z}, \sigma_x, \sigma_y, \sigma_z, I$. The possible magnetic point groups derived from this group can be found in reference 6. These groups contain the original elements of G and their combination with R , where R is the time-reversal element.⁷ The symmetry element R reverses magnetic moments and magnetic fields, and otherwise leaves the crystal invariant. In the orthoferrites, the center of inversion is through a magnetic ion, and therefore the element RI cannot exist for a magnetic state, leaving only the magnetic point groups containing I . Furthermore, if the magnetic cell is equal to the x-ray one, (as demonstrated by neutron diffraction³ for LaFeO_3) the element

* On leave of absence from the Weizmann Institute of Science, Rehovoth, Israel.

¹ R. Pauthenet and P. Blum, *Compt. rend.* **239**, 33 (1954); H. Forestier and G. Guiot-Guillain, *ibid.* **230**, 1844 (1950); M. A. Gilileo, *J. Chem. Phys.* **24**, 1239 (1956); R. M. Bozorth, V. Kramer, and J. P. Remeika, *Phys. Rev. Letters* **1**, 3 (1958); R. C. Sherwood, J. P. Remeika, and H. J. Williams, *J. Appl. Phys.* **30**, 217 (1959); H. Watanabe, *J. Phys. Soc. Japan* **14**, 511 (1959); C. Kuroda, T. Miyadai, A. Naemura, N. Niizeki, and H. Takata, *Phys. Rev.* **122**, 446 (1961); G. H. Jonker, *Physica* **22**, 707 (1956).

² S. Geller and E. A. Wood, *Acta Cryst.* **9**, 563 (1956); S. Geller, *J. Chem. Phys.* **24**, 1236 (1956).

³ W. C. Koehler and E. O. Wollan, *J. Phys. Chem. Solids* **2**, 100 (1957); W. C. Koehler, E. O. Wollan and M. K. Wilkinson, *Phys. Rev.* **118**, 58 (1960).

⁴ I. Dzyaloshinsky, *J. Phys. Chem. Solids* **4**, 241 (1958).

⁵ T. Moriya, *Phys. Rev.* **120**, 91 (1960).

⁶ B. A. Tavger and V. M. Zaitsev, *Soviet Phys.—JETP* **3**, 430 (1956).

⁷ L. D. Landau and E. M. Lifshitz, *Statistical Physics* (Pergamon Press, New York, 1958), p. 427.

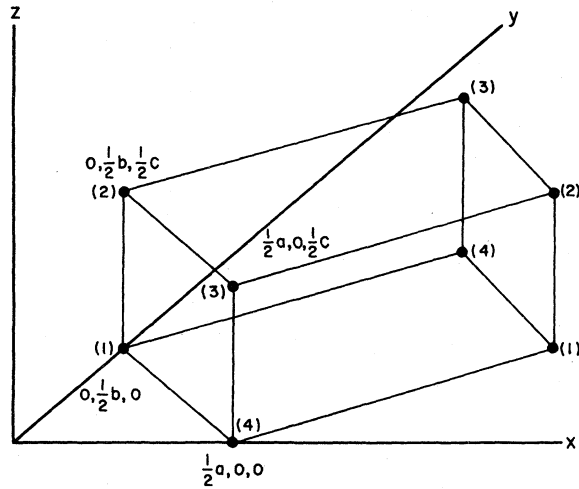


FIG. 1. Location of the Fe^{3+} ions in the unit cell of the orthoferrites.

I permutes only equivalent magnetic ions and is therefore equivalent to the identity operator with respect to the magnetic structure. In this case it is sufficient to consider only the magnetic point groups associated with the group⁸ $D_2 = E, C_{2x}, C_{2y}, C_{2z}$. These groups are $G_1 = E, C_{2x}, C_{2y}, C_{2z}$; $G_{2,3,4} = E, C_{2i}, RC_{2j}, RC_{2k}$, where i, j, k , stand for permutations of x, y, z . The rotation axes are all screw axes and there are four of each kind in the crystallographic unit cell, with coordinates

$$\begin{aligned} C_{2x}(y = \frac{1}{4}b; \frac{3}{4}b; z = 0; \frac{1}{2}c), \\ C_{2y}(x = \frac{1}{4}a; \frac{3}{4}a; z = \frac{1}{4}c; \frac{3}{4}c), \\ C_{2z}(x = 0; \frac{1}{2}a; y = 0; \frac{1}{2}b). \end{aligned}$$

The four nonequivalent magnetic ions are located at the points $S_1(0, \frac{1}{2}b, 0)$; $S_2(0, \frac{1}{2}b, \frac{1}{2}c)$; $S_3(\frac{1}{2}a, 0, \frac{1}{2}c)$; $S_4(\frac{1}{2}a, 0, 0)$ in the unit cell, as shown in Fig. 1. The element C_{2x} permutes site 2 and 3 and 1 with 4, C_{2y} permutes 1 with 3 and 2 with 4 and C_{2z} permutes 1 with 2 and 3 with 4. The magnetic moments transform like vectors under rotations and are reversed by R . Writing down the condition for the invariance of the magnetic crystal under the different symmetry operations, one finds that the above groups yield the following magnetic structures:

$$\begin{array}{ll} E, C_{2x}, C_{2y}, C_{2z}, & E, C_{2x}, RC_{2y}, RC_{2z}, \\ S_{1x} = -S_{2x} = -S_{3x} = S_{4x}, & S_{1x} = S_{2x} = S_{3x} = S_{4x}, \\ S_{1y} = -S_{2y} = S_{3y} = -S_{4y}, & S_{1y} = S_{2y} = -S_{3y} = -S_{4y}, \\ S_{1z} = S_{2z} = -S_{3z} = -S_{4z}; & S_{1z} = -S_{2z} = S_{3z} = -S_{4z}; \end{array}$$

$$\begin{array}{ll} E, RC_{2x}, C_{2y}, RC_{2z}, & E, RC_{2x}, RC_{2y}, C_{2z}, \\ S_{1x} = S_{2x} = -S_{3x} = -S_{4x}, & S_{1x} = -S_{2x} = S_{3x} = -S_{4x}, \\ S_{1y} = S_{2y} = S_{3y} = S_{4y}, & S_{1y} = -S_{2y} = -S_{3y} = S_{4y}, \\ S_{1z} = -S_{2z} = -S_{3z} = S_{4z}; & S_{1z} = S_{2z} = S_{3z} = S_{4z}; \end{array}$$

⁸ A. J. Heeger, O. Beckman and A. M. Portis, Phys. Rev. **123**, 1652 (1961).

where S_{ni} are the respective components of the n th ion.

These are all the possible magnetic structures for a magnetic unit cell that is equal to the x-ray one. The configurations described by Bozorth⁹ can be derived from these by further assuming the existence of only two sublattices. This additional restriction does not add to the symmetry of the magnetic structures which anyhow have the maximum symmetry possible, which is that of the crystal. In these crystals, a two-sublattice system is favored by the isotropic superexchange interaction.

With the exception of Sm^1 , all the rare-earth and yttrium orthoferrites have at room temperature a ferromagnetic component in the z directions. They, therefore, belong to the magnetic point group $E, RC_{2x}, RC_{2y}, C_{2z}, R\sigma_x, R\sigma_y, \sigma_z, I$.

3. TORQUE MEASUREMENTS AND SYMMETRY

The properties of a magnetic material at low static fields can be described by the coefficients of the series expansion of the free energy F in a power series in the applied field \mathbf{H} .

$$F = C_0 + \sum \sigma_i(0)H_i + \frac{1}{2} \sum \chi_{ij}H_iH_j + \sum C_{ijk}H_iH_jH_k + \dots,$$

where i, j, k stand for the coordinate axes. As shown below, one can use torque measurements, supplemented by susceptibility measurements, in order to evaluate experimentally the coefficients of the series expansion of F . The first term is irrelevant. The coefficients $\sigma_i(0)$ of the second term give the permanent magnetic moment of the crystal, the χ_{ij} are the terms of the usual susceptibility tensor, and can be collected into six constants. The C_{ijk} tensor will add detailed information on the mechanism that produces the spin configuration. These 27 terms can be bunched into 10 terms prior to any symmetry consideration.

The fact that the free energy must be invariant with respect to all the symmetry operations of the magnetic point group of the crystal, will further reduce the number of coefficients. The operator RC_{2x} leaves H_y and H_z unchanged, and reverses H_x so that only even powers in H_x can remain in the free energy expression. Similarly, RC_{2y} eliminates odd powers of H_y . As previously described, the inversion operator leaves the energy expression unchanged, and therefore does not introduce any restriction on it. All the other symmetry operators are redundant because they are generated by those mentioned above. It follows that the χ_{ij} tensor contains only the three terms χ_{ii} ,¹⁰ and the only nonvanishing C_{ijk} are the three terms $C_{xxx}, C_{yyz}, C_{zzz}$. The

⁹ R. M. Bozorth, Phys. Rev. Letters **1**, 362 (1958).

¹⁰ The χ_{ij} tensor is in general symmetric; therefore it can be always represented by three numbers only. The symmetry operations add only the information that its principal axes coincide with the crystallographic ones. From here on the double indexing χ_{ij} will be dropped and the susceptibilities written χ_x, χ_y, χ_z .

TABLE I. Coefficients of the energy series expansion evaluated from torque measurements.

Units	$\sigma_z(0)$ (emu/g)	From magnetization measurements			From torque measurements			$C_{zzz} \times 10^{12}$ (emu/g oe ²)	$C_{yyz} \times 10^{12}$ (emu/g oe ²)	$C_{zzz} \times 10^{12}$ (emu/g oe ²)	T_N (°K)	Mo- lecular weight (g)
		$10^6 \chi_x$ (emu/g oe)	$10^6 \chi_y$ (emu/g oe)	$10^6 \chi_z$ (emu/g oe)	$10^6(\chi_y - \chi_x)$ (emu/g oe)	$10^6(\chi_z - \chi_x)$ (emu/g oe)	$10^6(\chi_z - \chi_y)$ (emu/g oe)					
YFeO ₃	1.2	18	12	12.5	-7 ÷ -10	-7 ÷ -8	<0.1	-20 ÷ -25	<1	<1	648	193
LaFeO ₃	1.0	7.5	9	10.5	1.8	1.3	<0.1	12.5	-1.2 ÷ -1.7	-7.5	738	243
LuFeO ₃	1.0	0.8 ÷ 1.9	1.3	<0.1	9	<0.2	<2	...	279

free energy now takes the form

$$F = \sigma_z(0)H_z + \frac{1}{2} \sum \chi_i H_i^2 + C_{zzz} H_x^2 H_z + C_{yyz} H_y^2 H_z + C_{zzz} H_z^3 + \dots \quad (1)$$

The component σ_i of the total magnetization $\sigma(\mathbf{H})$ are given by¹¹ $\sigma_i = \partial F / \partial H_i$, yielding

$$\sigma_x = \chi_x H_x + 2C_{zzz} H_x H_z, \quad (2a)$$

$$\sigma_y = \chi_y H_y + 2C_{yyz} H_y H_z, \quad (2b)$$

$$\sigma_z = \sigma_z(0) + \chi_z H_z + C_{zzz} H_z^2 + C_{yyz} H_y^2 + 3C_{zzz} H_z^2. \quad (2c)$$

If one considers only fields parallel to the magnetization and in the principal directions, one gets

$$\begin{aligned} \sigma_x &= \chi_x H_x; & \sigma_y &= \chi_y H_y; \\ \sigma_z &= \sigma_z(0) + \chi_z H_z + 3C_{zzz} H_z^2. \end{aligned} \quad (3)$$

The torque components are given by $T_i = H_j \sigma_k - H_k \sigma_j$, or explicitly:

$$T_x = H_y [\sigma_z(0) + \chi_z H_z + 3C_{zzz} H_z^2 + C_{zzz} H_x^2 + C_{yyz} H_y^2] - H_z [\chi_y H_y + 2C_{yyz} H_y H_z], \quad (4)$$

$$T_y = H_z [\chi_x H_x + 2C_{zzz} H_x H_z] - H_x (\sigma_z(0) + \chi_z H_z + 3C_{zzz} H_z^2 + C_{yyz} H_y^2), \quad (5)$$

$$T_z = H_x [\chi_y H_y + 2C_{yyz} H_y H_z] - H_y [\chi_x H_x + 2C_{zzz} H_x H_z]. \quad (6)$$

4. EXPERIMENTAL

The torquemeter built¹² for these measurements was a high sensitivity automatic recording torque magnetometer similar to that described by Croft *et al.*,¹³ with a sensitivity of about 10^{-2} dyne cm. The magnetic field was continuously measured with a Rawson rotating coil gaussmeter, and curves of torque vs field plotted on an *x-y* recorder.

The linear part of the torque in the *X* and *Y* planes was several orders of magnitude larger than the contributions of the nonlinear terms and masked those completely. Therefore, the following technique was used: The crystals were mounted with the ferromagnetic *z* axis parallel to the axis of a coil rigidly connected to the lower end of the magnetometer. For the meas-

urement of the nonlinear terms the ferromagnetic component was bucked out by the current in the coil. This current was adjusted so that the slope of the torque curve as a function of field was zero at $H=0$. As the *z* axis of the crystal could not be perfectly aligned parallel to the axis of the coil, the current had to be slightly readjusted for different angles.

The single crystals were carefully selected, and only untwinned ones measured. They weighed between 5 and 100 mg. These crystals were grown by Remeika with the flux method.¹⁴ Tests on crystals of YFeO₃ of different degrees of purity showed that the magnetic properties studied varied only very slightly.

For reasons to be described below, the crystals were also selected for high coercive force, which was found to vary considerably from crystal to crystal, in general increasing with decreasing size. All the torque measurements were performed with the applied field normal to the torque, so that in the expression for T_i , the component $H_i=0$.

The constant σ_{0z} is evaluated either by a magnetization measurement in the *z* direction and extrapolating to $H_z=0$ following (3), or by torque measurements, by taking the slope of T_x as a function of H_y for low fields. It is seen from (4) that in this case T_x is not a function of the susceptibility, and only the third-order coefficient C_{yyz} appears. This coefficient is so small that the torque curve appears as a straight line up to fields of 20 koe. The susceptibility measurements were performed by Williams and Sherwood in a magnetometer described elsewhere.¹⁵

The sensitivity of the magnetometer is of the order of 10^{-3} emu, so that the accuracy of the susceptibility measurements is quite low. Therefore, one cannot use these values in order to evaluate the anisotropy of the susceptibility. On the other hand, the high sensitivity of the torquemeter, and the fact that torques are proportional to the difference in the susceptibility, yield a high sensitivity in the estimation of $\chi_i - \chi_j$. The precision here is probably determined by the accuracy of the geometrical alignment.

All the results are summarized in Table I. The constant C_{zzz} was evaluated from the torque component T_y as a function of H_x , see (5). The field was applied in this direction in order to exclude a contribution to the torque from the quadratic terms. How-

¹¹ L. D. Landau and E. M. Lifshitz, *Electrodynamics of Continuous Media* (Pergamon Press, New York, 1960), p. 147.

¹² The author wishes to thank W. D. Doyle and P. J. Flanders from the Franklin Institute for making available technical details concerning the magnetometer.

¹³ G. T. Croft, F. J. Donahoe, and W. F. Love, *Rev. Sci. Instr.* **26**, 360 (1955).

¹⁴ J. P. Remeika, *J. Am. Chem. Soc.* **78**, 4259 (1956).

¹⁵ R. M. Bozorth, H. J. Williams, and D. E. Walsh, *Phys. Rev.* **103**, 572 (1956).

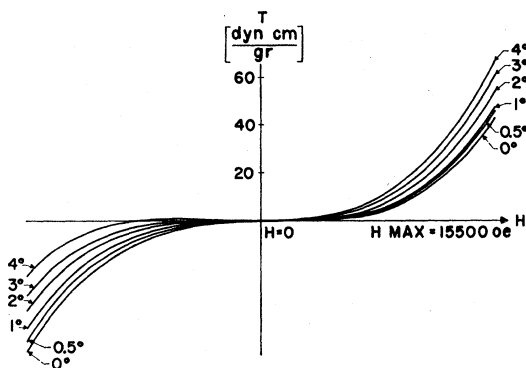


FIG. 2. Torque curves measured on an 0.1 g LaFeO_3 single crystal. The torque T_y is given as a function of field, for different orientations of the field in the Y plane. The angles shown are measured from the x axis. The absolute accuracy of the alignment is $\pm 2^\circ$. The relative accuracy is within 0.25%.

ever, because $\chi_z - \chi_x \gg HC_{zzz}$ for all practical fields, great accuracy was required in aligning the field parallel to the x axis.

Torque curves were therefore taken at different angles in the neighborhood of the x direction, with the field taking both positive and negative values. Exactly in the x direction one should get a curve antisymmetric in H . Deviating from x , one gets a mixing-in of the symmetric curve due to the $H_x H_z (X_x - X_z)$ term. This behavior is clearly demonstrated in the actual curves for LaFeO_3 , as shown in Figs. 2 and 3. When the H_z component exceeds the coercive force in the negative direction, the ferromagnetic component reverses irreversibly. One therefore needs crystals with a high coercive force, in order to allow negative excursions of the field large enough to enable an accurate determination of the symmetry of the torque curve.

From the curve which is nearest to antisymmetric, one finds the C_{zzz} coefficient. In the example shown in Fig. 2 this would be the curve denoted 1° . This curve fits remarkably well a cubic curve (as shown in Fig. 5).

The nonlinear terms in the torque are taken as positive if they have the same sign as the linear one.

The C_{yyz} constant is evaluated from T_x with $H = H_y$, see (4). The torque curve for LaFeO_3 is shown in Fig.

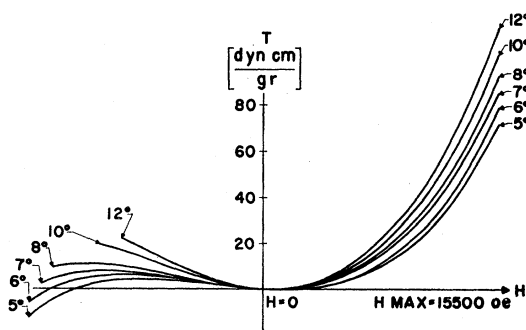


FIG. 3. See caption for Fig. 1.

4. The signal to noise ratio is rather low, however one can still see that the power dependence of the torque on H is higher than cubic. This is shown in Fig. 5, where the torque is drawn as a function of H^3 for $T_y(H = H_x)$ and $T_x(H = H_y)$. Approximating the curve of Fig. 4 by a cubic curve, one can roughly evaluate C_{yyz} . This is the value given in Table I. It is interesting to note that the linear term bucked out in this experiment is about 10^5 larger than the torques measured in Fig. 4.

Figure 6 shows T_x for LaFeO_3 as a function of field for different angles θ , ($\tan\theta = H_y/H_z$). The torques are very low, and only very rough estimates of $(\chi_z - \chi_y)$ and C_{zzz} could be made using (4). From measurements of T_z , one can evaluate $(\chi_y - \chi_x)$ using (6).

The results for LuFeO_3 were very similar in every respect to those of LaFeO_3 , and are given in Table I.

Measurements were done also on YFeO_3 which has the same crystal structure, and also has a ferromagnetic component in the z direction. The results of torque measurement, as shown in the table, differ from the

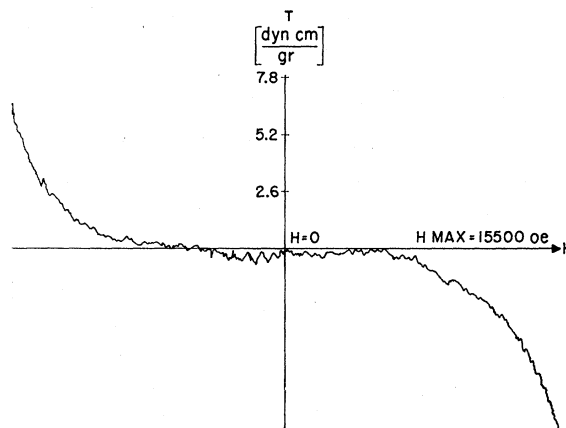


FIG. 4. Torque T_x as a function of field applied in the y direction, for the same crystal of Figs. 2 and 3.

other two materials in that C_{zzz} is here negative, and $(\chi_x - \chi_z) \approx (\chi_x - \chi_y) > 0$.

In principle C_{zzz} can be found also from measurements of the nonlinear component of σ_z as a function of H_z , as seen in (2). Magnetization measurements could in addition isolate the fourth-order terms D_{iii} . Unfortunately the lack of such a precision instrument prevented these measurements.

Within experimental error the extraneous constants C_{zzz} and C_{yyz} were found to be zero for the three crystals studied. The others were not evaluated.

5. CALCULATION OF THE COEFFICIENTS

In Sec. 3 symmetry considerations alone were used to find what independent constants were needed to describe the macroscopic magnetic properties of the crystals studied. The method of measuring these constants, and their actual measurements were de-

scribed in Sec. 4. No reference was made to the physical interactions, existing in these crystals, that are actually responsible for their spin configuration. In the introduction, two types of interactions that might be responsible for a canted spin structure were mentioned.

In this section the implications of these two different interaction mechanisms will be studied, and the magnetic tensors calculated for each of them.

As discussed in Sec. 2 a two-sublattice system is a reasonable approximation to the system studied. For simplicity in the mathematical analysis such a system will be assumed in all the following calculations. The molecular field approximation will be used throughout, and the magnitude of the spins will be assumed field independent.

The coefficients $\sigma_z(0)$, χ_i , C_{xxz} , C_{yyz} , C_{zzz} , for the two models, are calculated by expanding the components of the total magnetization in a series in the applied field, with the latter in the principal directions. Thus, using (2) one gets the following relations:

$$\begin{aligned} \chi_i &= d\sigma_i/dH_i, & C_{yyz} &= \frac{1}{2}d^2\sigma_z/dH_y^2, \\ C_{xxz} &= \frac{1}{2}d^2\sigma_z/dH_x^2, & C_{zzz} &= \frac{1}{6}d^3\sigma_z/dH_z^3, \end{aligned} \quad (7)$$

with the derivatives calculated at $H=0$. In all these cases, although there are two sublattices, the total free energy is a function of at most two independent geometrical parameters. The energy is minimized with respect to these parameters yielding the equilibrium equations. The magnetization components are expressed as a function of the two independent parameters, and therefore the derivatives (7) will be a function of the independent parameters and their derivatives with respect to H , calculated at $H=0$. These in turn are found from the equilibrium equations.

In the single ion magnetocrystalline anisotropy model the following interactions are assumed:

1. Isotropic superexchange with energy, $E_x = \lambda \sigma_1 \cdot \sigma_2$, where λ is a positive molecular field constant and σ_1 , σ_2 the magnetization vectors of the two sublattices. ($\sigma = \sigma_1 + \sigma_2$).
2. Energy of interaction with the applied field, $E_H = -\mathbf{H} \cdot (\sigma_1 + \sigma_2)$, where \mathbf{H} is the applied field.
3. Magnetocrystalline anisotropy energy,

$$E_k = K(\sin^2\delta_1 + \sin^2\delta_2).$$

Here K is the magnetocrystalline anisotropy constant and δ is the angle between the magnetization and the preferred crystallographic direction of magnetization of the appropriate sublattice. The symmetry of the crystal requires the value of the constant K to be equal for the two sublattices, and the preferred directions to be in symmetrical positions in the Y plane. Furthermore the fact that the ferromagnetic component at zero applied field is in the z direction, restricts the angle α between the preferred directions and the x axis to $\alpha \leq \pi/4$.

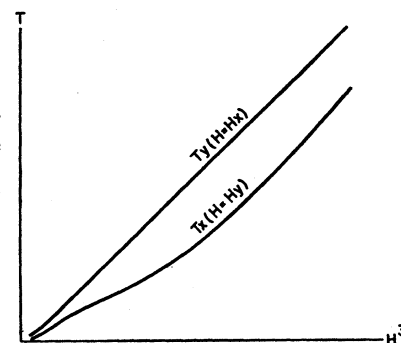


Fig. 5. Curve 1° of Fig. 2, (T_y), and the curve of Fig. 4, (T_x) plotted as a function of H^3 .

In the antisymmetric exchange interaction model the following interactions are assumed:

1. Isotropic superexchange.
2. Interaction with the applied field.

These two have the same form as previously described.

3. Magnetocrystalline anisotropy energy, with easy direction of magnetization equal for both sublattices and parallel to the x axis.

4. Antisymmetric exchange interaction with energy⁵ $E_d = -\mathbf{D} \cdot \sigma_1 \times \sigma_2$, where \mathbf{D} is a constant vector parallel to the y axis.

The coefficients are calculated in the appendix. All the results are collected in Table II. In the table, $H_a = 2K/\sigma_0$ where $\sigma_0 = |\sigma_1| = |\sigma_2|$. $H_e = \lambda\sigma_0$, $H_d = D\sigma_0$ and $H_b = 2K_b/\sigma_0$ where K_b is the anisotropy constant in the antisymmetric exchange model. γ_0 is the canting angle at $H=0$. For $\gamma_0 \ll 1$ it is given by

$$\gamma_0 = H_a(\sin 2\alpha)/4H_e. \quad (8)$$

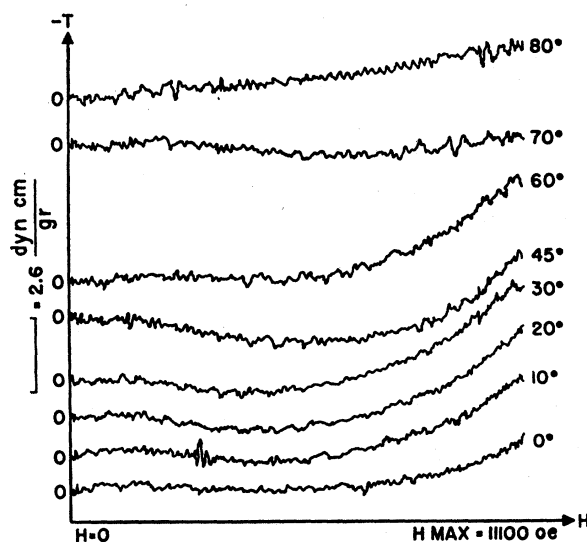


Fig. 6. Torque T_x as a function of field applied in different directions in the X plane. The angles are measured from the y axis.

TABLE II. Calculated values of the coefficients of the energy series expansion according to the two models studied. The expressions are correct within the approximation $\gamma_0 \ll 1$.

	Single-ion anisotropy model	Antisymmetric exchange model
$\sigma_z(0)$	$\sigma_0 H_a \sin 2\alpha / 2H_e$	$\sigma_0 H_a / H_e$
χ_x	$\sigma_0 H_a \sin^2 2\alpha / 8H_e^2 \cos 2(\alpha - \gamma_0)$	$\sigma_0 H_a^2 / 2H_b H_e^2$
χ_y	σ_0 / H_e	σ_0 / H_e
χ_z	σ_0 / H_e	σ_0 / H_e
C_{xxx}	$\sigma_0 \sin 2\alpha [\cos(2\alpha - \gamma_0) - H_a \sin^2 2\alpha / 16H_e]$	$\sigma_0 H_a (1 - H_a^2 / 4H_b H_e) / 2H_b H_e^2$
C_{yyy}	$4H_e^2 \cos^2 2(\alpha - \gamma_0)$	
C_{zzz}	$-\sigma_0 H_a \sin 2\alpha / 16H_e^3$	$-\sigma_0 H_a / 8H_e^3$
	$-\sigma_0 \sin 2\alpha / 8H_e^2$	$-\sigma_0 H_a / 8H_e^3$

6. CALCULATED VS EXPERIMENTAL RESULTS, DISCUSSION AND CONCLUSION

In this section an attempt will be made to establish which of the two mechanisms studied is predominant in causing weak ferromagnetism in the orthoferrites. This will be done by comparing the measured coefficients with those calculated according to the two models. From this comparison, the parameters involved in the two models will also be evaluated.

In reality both mechanisms considered will usually exist simultaneously, and therefore a quantitative comparison between experimental values and those calculated according to the distinct models is of doubtful value. One must look for qualitative difference in the behavior of the calculated coefficients to decide with any degree of confidence which interaction is predominant.

Consider first the calculated coefficients χ_y^k , χ_y^d , χ_x^k , χ_x^d . (The added superscript k or d stands here and in the following discussion for the value calculated according to the single ion anisotropy or antisymmetric exchange model respectively, according to Table II. Coefficients without an added superscript are reserved for the experimental values as given in Table I.) These four coefficients are equal within $\sin \gamma_0$ or about 1% and will be denoted simply χ_1 . The value of $(\chi_y - \chi_x) / \chi_y$ as measured by torque measurements (which measure the difference directly), was below the noise level, the upper limit being of the order of 1% which is in agreement with the calculated value. The constant χ_1 is equal to the transverse susceptibility λ^{-1} of a regular antiferromagnet, which is temperature independent below the Néel temperature.¹⁶

On the other hand, consider the susceptibility in the x direction. If the canting angle of the spins is small, in addition to the terms χ_x^k or χ_x^d there is a comparable paramagnetic contribution, χ_x^p , which increases with temperature more strongly than linearly, reaching χ_1 at the Néel temperature.¹⁷ As the Néel temperatures of

YFeO₃ and LaFeO₃ are 375°C and 465°C, respectively,^{3,18,19} the contribution χ_x^p to χ_x will be less than $\frac{1}{2}\chi_1$ at room temperature.

The calculated ratio χ_x^k / χ_1 , taken from Table II, is

$$\chi_x^k / \chi_1 = H_a \sin^2 2\alpha / 8H_e \cos 2(\alpha - \gamma_0). \quad (9)$$

As previously mentioned, $\alpha \leq \pi/4$, so that using (8), one finds from (9)

$$\chi_x^k / \chi_1 \leq H_a \sin^2 2\alpha / 8H_e \sin 2\gamma_0 \approx \frac{1}{4}. \quad (10)$$

As $\chi_x^p / \chi_1 \leq \frac{1}{2}$ at room temperature, one expects, according to the single ion anisotropy model, a measured value of $\chi_x / \chi_1 < 1$, where χ denotes the measured value of χ_1 . On the other hand

$$\chi_x^d / \chi_1 = H_a^2 / 2H_e H_b,$$

and this ratio will be greater than unity if

$$H_a^2 > 2H_e H_b. \quad (11)$$

Now consider C_{xxx} . The question is, can this constant attain negative values? As seen from Table II, the sign of C_{xxx}^k is determined by the sign of the term S

$$S = \cos(2\alpha - \gamma_0) - H_a \sin^2(2\alpha / 16H_e).$$

Using (8) one gets

$$S = \cos(2\alpha - \gamma_0) - \sin \gamma_0 \sin 2\alpha / 4,$$

and as $\alpha \leq \pi/4$, one finds $S > 0$. Therefore, according to the single-ion anisotropy model, C_{xxx}^k is always positive. On the other hand, Table II shows that C_{xxx}^d will be negative for

$$H_a^2 > 4H_e H_b. \quad (12)$$

This basic difference in the behavior of the two models distinguishes between the two mechanisms without resorting to precise quantitative considerations.

Comparison of (11) and (12) shows that the conditions for obtaining $\chi_x^d > \chi_1$ and $C_{xxx}^d < 0$ are very similar, both requiring a low anisotropy in the Y plane.

The different behavior of the two mechanisms can be easily understood from the following arguments:

¹⁶ M. A. Gilleo, Phys. Rev. **109**, 777 (1958).

¹⁶ T. Nagamiya, K. Yosida, and R. Kubo, *Advances in Physics*, edited by N. F. Mott (Taylor and Francis Ltd., London, 1955), Vol. 4, p. 1.

¹⁷ R. M. Bozorth, *Ferromagnetism* (D. Van Nostrand Company Inc., Princeton, New Jersey, 1959), p. 472.

¹⁹ W. Roth, Pittsburg Diffraction Conference, 1954 (unpublished).

In the antisymmetric exchange model the weak ferromagnetism is the result of H_d alone, and this interaction is isotropic in the plane normal to the \mathbf{D} vector. The anisotropy in this plane is represented by H_b . As the weak ferromagnetic component is independent of H_b , in the limit of low anisotropy the canted spin system may be regarded as rigidly rotating in the Y plane, under the action of an applied field in the x direction. In this case it is obvious that C_{xxx} is negative, and χ_x proportional to H_b^{-1} .²⁰

In the single ion anisotropy model, the anisotropy is responsible for both the ferromagnetic component and the anisotropy in the Y plane. It is this interdependence that limits χ_x to values smaller than χ_1 and, C_{xxx} to positive values.

From Table I it is seen that for YFeO_3 , C_{xxx} is negative and $\chi_x > \chi$ showing that the predominant mechanism is in fact the antisymmetric exchange interaction.

The interaction fields will now be calculated for YFeO_3 from the measured coefficients.

From

$$\sigma_z(0)/\chi = H_d, \quad (13)$$

one finds $H_d = 10^5$ oe. Substituting this value in

$$C_{xxx}/\sigma_z(0) = (1 - H_d^2/4H_eH_b)/2H_eH_b, \quad (14)$$

one gets $2H_eH_b = 0.45 \times 10^{10}$ oe². As a check for consistency, the values of H_d and H_eH_b are substituted in the expression

$$\chi_x^d/\chi_1 = H_d^2/2H_eH_b, \quad (15)$$

yielding $\chi_x^d/\chi_1 = 2.2$, as compared to a measured ratio of between 1 and 1.5 depending on the paramagnetic contribution to χ_x . Taking into account the low precision of the measurements, this is good agreement.

In order to evaluate H_e and H_b one needs the sublattice saturation magnetization σ_0 . Assuming a moment of $5\mu_B$ per Fe^{++} ion one gets $\sigma_0 = 72$ emu/g.

From $\chi = \sigma_0/H_e$ one finds $H_e = 6 \times 10^6$ oe, $H_b = 370$ oe. The calculated coefficients C_{yyz}^d and C_{zzz}^d are of the order of 10^{-14} oersted⁻² emu/g⁻¹, definitely below the experimental upper limit.

The results of the measurements on LaFeO_3 are similarly treated: One gets

$$\sigma_0 = 57 \text{ emu/g}, \quad H_e = 6 \times 10^6 \text{ oe}, \quad H_d = 10^5 \text{ oe}.$$

Because C_{xxx} is positive for LaFeO_3 , (14) yields two results:

$$(2H_eH_b)_1 = 0.53 \times 10^{10} \text{ oe}^2, \quad (2H_eH_b)_2 = 7.7 \times 10^{10} \text{ oe}^2,$$

which in turn, using (15), yield the values

$$\begin{aligned} (\chi_x^d/\chi_1)_1 &= 1.9, & (H_b)_1 &= 450 \text{ oe}, \\ (\chi_x^d/\chi_1)_2 &= 0.13, & (H_b)_2 &= 6500 \text{ oe}. \end{aligned}$$

Both torque and susceptibility measurements show

that $\chi_x < \chi$; one is therefore forced to accept for H_b the high value of 6500 oe.

Because H_e and H_d are almost identical for YFeO_3 and LaFeO_3 , and both crystals have high Néel temperatures, the predominant mechanism is most likely the same in both materials.²¹

The high value of H_b in LaFeO_3 as compared to that of YFeO_3 is surprising. The iron lattice in YFeO_3 is much more distorted than in LaFeO_3 , but the magneto-crystalline anisotropy is probably caused by the distortion of the oxygen octahedra surrounding the iron ions,²² so that it appears that although the iron lattice in LaFeO_3 is less distorted than in YFeO_3 , the oxygen octahedra are more distorted. A refined x-ray study of these materials could probably clarify this question.

In view of this difficulty in LaFeO_3 it is interesting to analyze the experimental results on this material, in terms of the single-ion anisotropy model.

One finds, using Table II,

$$H_a \sin 2\alpha = 2\sigma_z(0)/\chi = 2 \times 10^5 \text{ oe}. \quad (16)$$

and from the relation $\sin \gamma_0 = \sigma_z(0)/2\sigma_0$, with $\sigma_0 = 57$ emu one gets

$$\gamma_0 \approx 0.009. \quad (17)$$

Consider now the following relation obtained from Table II

$$\sigma_z(0)/\chi_x^k = 4H_e \cos 2(\alpha - \gamma_0)/\sin 2\alpha > 4H_e \sin 2\gamma_0. \quad (18)$$

Using (8) and (16), (18) becomes

$$\sigma_z(0)/\chi_x^k > 2H_a \sin 2\alpha = 4 \times 10^5 \text{ oe}. \quad (19)$$

This equation serves as a check for the model. According to it, one expects

$$\chi_x^k \leq \sigma_z(0)/2H_a = 2.5 \times 10^{-6}, \quad (20)$$

where the equality holds for $\alpha = \pi/4$. From Table I one finds the total susceptibility in the x direction to be, at room temperature 7.4×10^{-6} . Even allowing for the paramagnetic contribution, one finds a susceptibility that exceeds the upper limit allowed by (20). Still, let this upper limit be assigned to $(\chi_x - \chi_{xp})$; this means $\alpha = \pi/4$ and from (16) one gets $H_a = 2 \times 10^5$ oe. Substituting these values in the expression for the other coefficients, one gets:

$$\begin{aligned} C_{xxx}^k &= 9 \times 10^{-12}; & C_{yyz}^k &= -0.3 \times 10^{-14}; \\ C_{zzz}^k &= -0.2 \times 10^{-12}. \end{aligned}$$

These results can be summarized as follows: According to the single ion crystal anisotropy model, one finds $H_a = 2 \times 10^5$ oe, which is equivalent to an anisotropy constant

²¹ The experimental values of C_{yyz} and C_{zzz} cannot be accounted for in LaFeO_3 . However it must be remembered that their evaluation is very rough, as the torques are very low.

²² J. J. Pearson, Phys. Rev. **121**, 695 (1961).

²⁰ This explanation has been pointed out by F. Keffer.

$$K = \frac{1}{2}\sigma_0 H_a = 6 \times 10^6 \text{ erg/g} = 4.3 \times 10^{-15} \text{ erg/ion} \\ = 25 \text{ cm}^{-1}.$$

This value seems very large for a trivalent iron ion.²³

The fact that $\alpha \approx \pi/4$ suggests that it should be possible to flip the ferromagnetic component in the x direction with relative ease, at least with a suitable heat treatment. However, all attempts in this direction gave negative results.

The measured value of χ_x was found to be above the upper limit set by the model, and the agreement of the measured constants C_{yyz} and C_{zzz} with these calculated according to the single-ion anisotropy model is not any better than in the antisymmetric exchange model.

One can therefore conclude that both in YFeO_3 and LaFeO_3 the predominant mechanism responsible for weak ferromagnetism is the antisymmetric exchange interaction. The results of LuFeO_3 are so similar to these of LaFeO_3 that the same conclusions can be drawn for both.

Additional evidence as to the predominant mechanism can be obtained by magnetic resonance experiments, however the interpretation of these is not as straightforward as the torque measurements, especially in view of the fact that the zero field resonance lies in the submillimeter region, and one has to apply external fields of the order of²⁴ 150koe in order to reduce the resonance frequency to practical values.

ACKNOWLEDGMENTS

The author wishes to express his gratitude to J. P. Remeika for supplying the crystals, to H. J. Williams and R. C. Sherwood for performing the susceptibility measurements, and to S. Geller and S. Shtrikman for helpful discussions.

Finally the author is greatly indebted to S. Alexander for clarifying several points connected with the symmetry properties of crystals, and for reading and correcting the manuscript.

APPENDIX: CALCULATION OF THE COEFFICIENTS

The various interactions assumed for the two models studied, and the approximations used, are discussed in Sec. 5. Here only the mathematical derivation of the coefficients will be given.

A. Single Ion Magnetocrystalline Anisotropy Model

1. Field in the Y Plane

In this case, at equilibrium, the two magnetization vectors lie in the Y plane. The various directions and

²³ For Mn^{++} , which has the same electronic configuration, Pearson (see reference 22) gets an anisotropy of the order of 10^{-18} erg, while even for Ni^{++} , for which one would expect a higher anisotropy, Moriya [Phys. Rev. **117**, 635 (1960)] estimates in NiF_2 a value of only 2.5×10^{-16} erg.

²⁴ The author is indebted to S. Foner for carrying out preliminary resonance experiments on YFeO_3 .

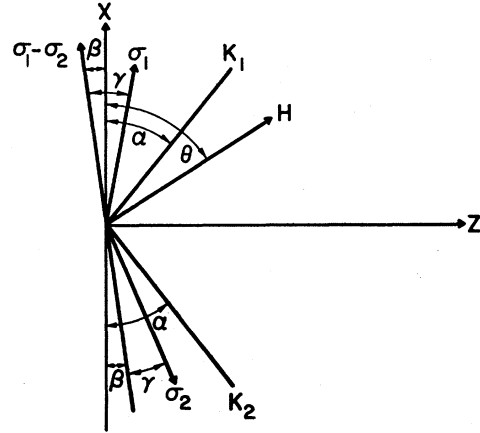


FIG. 7. Schematic diagram of the equilibrium state for fields applied in the Y plane. The anisotropy easy directions are in the Y plane.

angles used in the following, are shown in Fig. 7. Expressing the energy as a function of β , the angle between $(\sigma_1 - \sigma_2)$, and the x axis, γ the angle between σ_1 and $(\sigma_1 - \sigma_2)$, and θ , the angle between \mathbf{H} and the x axis, and minimizing it with respect to the two variables β, γ , one gets the equilibrium equations²⁵:

$$2h \sin \gamma \cos(\theta + \beta) - \sin 2\beta \cos 2(\alpha - \gamma) = 0, \quad (21)$$

$$2h \cos \gamma \sin(\theta + \beta) + \cos 2\beta \sin 2(\alpha - \gamma) - 2g \sin 2\gamma = 0, \quad (22)$$

where

$$h = H/H_a, \quad H_a = 2K/\sigma_0, \quad \sigma_0 = |\sigma_1| = |\sigma_2|, \\ g = H_e/H_a, \quad H_e = \lambda\sigma_0. \quad (23)$$

The angle of canting, γ_0 , at $h=0$ is found by substituting $h=\beta=0$ in (22) yielding

$$\tan 2\gamma_0 = \sin 2\alpha / (2g + \cos 2\alpha).$$

As the exchange field in these materials is of the order of 10^6 – 10^7 oe, as shown by the high Néel temperature, one can safely assume $g \gg 1$ and therefore

$$\gamma_0 \approx \sin 2\alpha / 4g = H_a \sin 2\alpha / 4H_e. \quad (24)$$

In the three crystals measured it was found that γ_0 is of the order of 10^{-2} so that (24) is fully justified. In the following the symbol \approx will mean that (24) was used.

a. Field in the x direction. In this case $\theta=0$, and one can eliminate β from (21) and (22) getting

$$h_x^2 = \cos^2 2(\alpha - \gamma) [2g \sin 2\gamma - \sin 2(\alpha - \gamma)] / \\ [\sin 2\alpha - \sin 2(\alpha - \gamma)]. \quad (25)$$

²⁵ The equilibrium state described in Eqs. (21) and (22) and schematically shown in Fig. 7 may stop being stable at high fields. The field at which this actually occurs depends on the angle α , but is in general of the order of magnitude of $(H_e H_a)^{1/2}$; however, for all values of H used experimentally in the evaluation of the coefficients this equilibrium is the only stable one.

The total magnetization component σ_x in the x direction is

$$\sigma_x = 2\sigma_0 \sin\gamma \sin\beta,$$

and substituting $\sin\beta$ from (21) with $\theta=0$, one gets

$$\sigma_x = 2\sigma_0 h_x \sin^2\gamma / \cos 2(\alpha - \gamma). \quad (26)$$

The magnetization is now expanded in a series in h_x at $h_x=0$.

$$\sigma_x = \sigma_x(0) + \sigma_x' h_x + \frac{1}{2} \sigma_x'' h_x^2 + \dots,$$

where the primes denote, here and in all the subsequent equations, derivatives with respect to the component of the reduced field h considered, at $h_i=0$.

From (26) one finds

$$\sigma_x' = 2\sigma_0 \sin^2\gamma_0 / \cos 2(g - \gamma_0), \quad (27)$$

and from (7), (27), and (24)

$$\chi_x = \frac{d\sigma_x}{dH_x} = \frac{\sigma_x'}{H_a} \approx \frac{\sigma_0 H_a \sin^2 2\alpha}{8H_e^2 \cos 2(\alpha - \gamma_0)}. \quad (28)$$

Similarly

$$\begin{aligned} \sigma_z &= 2\sigma_0 \sin\gamma \cos\beta \\ &= 2\sigma_0 \sin\gamma [1 - (h_x \sin\gamma / \cos 2(g - \gamma))^2]^{\frac{1}{2}}, \end{aligned} \quad (29)$$

with

$$\sigma_z(0) = 2\sigma_0 \sin\gamma_0 \approx \sigma_0 H_a \sin 2g / 2H_e,$$

and using (7), (25), (29), and (24) one finds

$$C_{zzz} = \frac{\sigma_0 \sin 2\alpha}{4H_e^2 \cos^2 2(\alpha - \gamma)} \left[\cos(2\alpha - \gamma_0) - \frac{H_a \sin^2 2\alpha}{16H_e} \right].$$

b. Field in the z direction. Here $\theta = \pi/2$, $\beta = 0$. Substituting these values in (22), one gets

$$h_x = [2g \sin 2\gamma - \sin 2(g - \gamma)] / 2 \cos\gamma. \quad (30)$$

The magnetization in the z direction is

$$\sigma_z = 2\sigma_0 \sin\gamma, \quad (31)$$

and with (30)

$$\sigma_z' = 2\sigma_0 \cos^2\gamma_0 [2g \cos 2\gamma_0 + \cos 2(\alpha - \gamma_0)]. \quad (32)$$

Using (7) and (24) one gets

$$\chi_z = \sigma_z' / H_a \approx \sigma_0 / H_e.$$

From (30) and (31) one finds

$$\sigma_z'' = -3\sigma_0 \sin 2\gamma_0 \cos\gamma_0 / [2g \cos 2\gamma_0 + \cos 2(\alpha - \gamma_0)], \quad (33)$$

and with (7) and (24)

$$C_{zzz} = \sigma_z'' / 6H_a^2 \approx -\sigma_0 \sin 2\alpha / 8H_e^2.$$

2. Field in the y Direction

The last coefficients that remain to be calculated are χ_y and C_{yyz} . These will be calculated by applying the field in the y direction. The equilibrium state for this

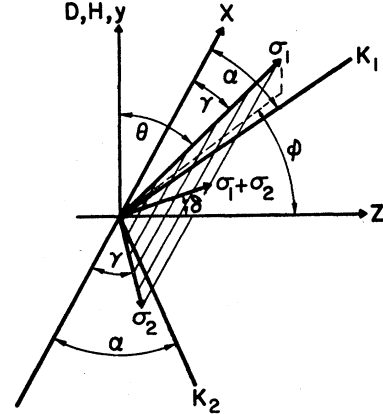


FIG. 8. Schematic diagram of the equilibrium state for fields applied in the y direction. The anisotropy easy directions are in the Y plane.

case is schematically shown in Fig. 8, where δ is the angle between $(\sigma_1 + \sigma_2)$ and the z axis.

The reduced energy e is now

$$\begin{aligned} e &= E/2K = -g \cos 2\gamma - 2h_y \sin\gamma \sin\delta \\ &\quad - (\cos\gamma \cos\alpha + \sin\gamma \sin\alpha \cos\delta)^2. \end{aligned} \quad (34)$$

Minimizing e with respect to δ and γ , one gets the equilibrium equations,

$$\begin{aligned} g \sin 2\gamma - h \cos\gamma \sin\delta \\ - \sin\gamma \cos\gamma (\cos^2\delta \sin^2\alpha - \cos^2\alpha) \\ - \sin\alpha \cos\alpha \cos\delta \cos 2\gamma = 0, \end{aligned} \quad (35)$$

$$h \cos\delta - \sin\alpha \sin\delta \times (\cos\gamma \cos\alpha + \sin\gamma \sin\alpha \cos\delta) = 0. \quad (36)$$

The magnetization in the z direction is given by

$$\sigma_z = 2\sigma_0 \sin\gamma \cos\delta. \quad (37)$$

Using the fact that at $h_y=0$

$$\gamma = \gamma_0, \quad \delta = 0, \quad \gamma' = 0, \quad (38)$$

one finds from (37)

$$\sigma_z'' / 2\sigma_0 = (\cos\gamma_0)\gamma'' - (\sin\gamma_0)\delta'^2. \quad (39)$$

Taking the derivative of (36) with respect to h and using (38), one finds

$$\delta' = [\sin\alpha \cos(\alpha - \gamma_0)]^{-1}, \quad (40)$$

and taking the second derivative of (35), using (40), one gets

$$\begin{aligned} \gamma'' = \sin\alpha \cos\alpha / \sin^2\alpha \cos^2(\alpha - \gamma_0) \\ \times [2g \cos 2\gamma_0 + \cos 2(\alpha - \gamma_0)]. \end{aligned} \quad (41)$$

Substituting (40) and (41) in (39) and using (24), one gets

$$\sigma_z'' \approx -\sigma_0 \sin 2\alpha / 8g^3, \quad (42)$$

and from (7)

$$C_{yyz} = \sigma_z'' / 2H_a^2 \approx -\sigma_0 H_a \sin 2\alpha / 16H_e^3.$$

In order to find χ_y one writes

$$\sigma_y = 2\sigma_0 \sin\gamma \sin\delta. \quad (43)$$

Using (28) and (40) in (43), one finds

$$\sigma_y' = 2\sigma_0 \sin\gamma_0 [\sin\alpha \cos(\alpha - \gamma_0)]^{-1}, \quad (44)$$

and from (7) and (24)

$$\chi_y \approx \sigma_0 / H_e.$$

B. Antisymmetric Exchange Model

1. Field Parallel to the x Axis

Using the same notation as in the previous paragraph, the free energy is

$$e = E/2K_b = -g \cos 2\gamma - d \sin 2\gamma - 2h_x \sin\gamma \sin\beta - \frac{1}{2} \cos 2\beta \cos 2\gamma, \quad (45)$$

where

$$g = H_e/H_b, \quad H_b = 2K_b/\sigma_0, \quad h = H/H_b, \\ d = H_d/H_b, \quad H_d = D\sigma_0, \quad (46)$$

and K_b is the anisotropy constant. (The easy direction is parallel to the x axis.) Minimizing e with respect to β and γ one gets the two equilibrium equations. Here also the equilibrium is stable for all practical values of applied field. From one equation one finds

$$\sin\beta = h \sin\gamma / \cos 2\gamma, \quad (47)$$

and by eliminating β from the other one gets

$$h_x^2 = \cos^2(2\gamma) [1 + 2(d^2 + g^2)^{\frac{1}{2}} \sin(2\gamma + \epsilon) (\sin 2\gamma)^{-1}], \quad (48)$$

where

$$\tan\epsilon = -d/g.$$

One also finds

$$\tan 2\gamma_0 = d/(g + \frac{1}{2}). \quad (49)$$

In this model too, one can safely assume $\gamma \ll 1$ so that, with the assumption $g \gg 1$

$$\gamma_0 \approx d/2g = H_b/2H_e. \quad (50)$$

The constants $\sigma_z(0)$ and C_{xxx} are found by writing [using (47)]

$$\sigma_z = 2\sigma_0 \sin\gamma \cos\beta = 2\sigma_0 \sin\gamma \\ \times [1 - (h_x \sin\gamma / \cos 2\gamma)^2]^{\frac{1}{2}}. \quad (51)$$

With (50) one gets

$$\sigma_z(0) = 2\sigma_0 \sin\gamma_0 \approx \sigma_0 H_d / H_e,$$

and from (51), (48), (50), and (7) C_{xxx} is found to be

$$C_{xxx} = \frac{1}{2} \sigma_z'' / H_b^2 \approx \sigma_0 H_d [1 - H_d^2 / 4H_e H_b] / 2H_e^2 H_b.$$

Using (47) one gets

$$\sigma_x = 2\sigma_0 \sin\gamma \sin\beta = 2\sigma_0 h_x \sin^2\gamma / \cos 2\gamma,$$

and with (7) and (50)

$$\chi_x = \sigma_x' / H_b \approx \sigma_0 H_d^2 / 2H_e^2 H_b.$$

2. Applied Field Parallel to y Axis

The angles defining the equilibrium state in this case are shown in Fig. 8. Using the same notation as in the preceding paragraphs, one finds:

$$E_d = -\sigma_0 H_d \cos\delta \sin 2\gamma; \quad E_x = -H_e \sigma_0 \cos 2\gamma; \\ E_k = -2K_b \cos^2\gamma,$$

and in terms of the magnetization coordinates (θ, φ) , (neglecting constant terms) one gets the following expressions:

$$E_d = -H_d \sigma_0 \sin^2\theta \sin 2\varphi, \\ E_x = -2H_e \sigma_0 \sin^2\theta \sin^2\varphi, \\ E_k = -2K_b \sin^2\theta \sin^2\varphi, \\ E_H = -2H\sigma_0 \cos\theta.$$

The reduced free energy is therefore

$$e = E/2K_b = -2h \cos\theta - d \sin^2\theta \sin 2\varphi - (2g+1) \sin^2\theta \sin^2\varphi. \quad (52)$$

From the equilibrium equations obtained by minimizing e with respect to φ , and θ one finds

$$\sin\varphi = \text{const} = \cos\gamma_0, \quad (53)$$

$$\cos\theta = h_y \cdot f(\gamma);$$

$$f(\gamma) = [d \sin 2\gamma_0 + (2g+1) \cos^2\gamma_0]^{-1}. \quad (54)$$

Substituting (54) in

$$\sigma_y = 2\sigma_0 \cos\theta,$$

one gets, using (50) and (7),

$$\chi_y = \sigma_y' / H_b \approx \sigma_0 / H_e.$$

In order to find C_{yyz} we write, using (53) and (54),

$$\sigma_z = 2\sigma_0 \sin\theta \cos\varphi = 2\sigma_0 \sin\gamma_0 [1 - h_y^2 f^2(\gamma_0)]^{\frac{1}{2}}, \quad (55)$$

which in turn yields

$$\sigma_z'' = -2\sigma_0 \sin\gamma_0 f^2(\gamma_0). \quad (56)$$

Using (7) and (50) one gets from (56)

$$C_{yyz} = \sigma_z'' / 2H_b^2 \approx -\sigma_0 H_d / 8H_e^3.$$

3. Field in the z Direction

In this case $\theta = \pi/2$ and $E_H = -2H\sigma_0 \cos\varphi$, and using the relation $\sin\varphi = \cos\gamma$ one gets for the free energy

$$e = -d \sin 2\gamma - 2h \sin\gamma - (2g+1) \cos^2\gamma. \quad (57)$$

Minimizing e with respect to γ yields

$$h = [(g + \frac{1}{2}) \sin 2\gamma - d \cos 2\gamma] / \cos\gamma. \quad (58)$$

The coefficients χ_z and C_{zzz} are found from σ_z

$$\sigma_z = 2\sigma_0 \cos\varphi = 2\sigma_0 \sin\gamma. \quad (59)$$

Taking the derivatives of (59) using (58) with (7) and (50) one gets

$$\chi_z = \sigma_z' / H_b \approx \sigma_0 / H_e,$$

$$C_{zzz} = \sigma_z'' / 6H_b^2 \approx -\sigma_0 H_d / 8H_e^3.$$

It can be easily verified that for both models, all the third-order coefficients apart from these calculated here,

are actually zero, as required by the symmetry of the crystal.

With the same technique one can also calculate the coefficients of the higher-power terms in the energy expansion. However, there is no point in doing this inasmuch as the experimental technique is not refined enough to measure these constants.

Paramagnetic Resonance of Ni^{2+} and Ni^{3+} in TiO_2 †

HENDRIK J. GERRITSEN* AND EDWARD S. SABISKY
RCA Laboratories, Princeton, New Jersey
(Received November 14, 1961)

Electron spin resonance was observed in nickel-doped rutile. The majority of the nickel is in the divalent state, and probably occupies an interstitial position. The parameters describing the Ni^{2+} spectra are: $S=1$; $g[\bar{z}]=2.20$; $g[\bar{y}]=g[\bar{x}]=2.10$; $D=-8.3 \text{ cm}^{-1}$; and $|E|=0.137 \text{ cm}^{-1}$ at 4.2°K . Some of the nickel, also probably occupying an interstitial position, is in the trivalent state, as was verified by oxidation-reduction tests. The parameters are: $S=\frac{1}{2}$ and $g[\bar{z}]=2.254$; $g[\bar{c}]=2.085$; $g[\bar{x}]=2.084$. A third spectrum due to nickel in an unknown valence state appears after the sample is illuminated. It represents nickel in a substitutional site with $S=\frac{1}{2}$ and $g[\bar{1}10]=2.272$; $g[\bar{c}]=2.237$; $g[\bar{1}\bar{1}0]=2.050$.

I. INTRODUCTION

THE paramagnetic resonance of rutile, TiO_2 , containing 0.01% nickel grown at RCA Laboratories by M. Kestigan and E. Aleshin, was investigated.

Three distinctly different spectra were observed, which will be discussed separately. Afterwards data on the interrelationship and explanation of these spectra as also a comparison with copper- and cobalt-doped rutile will be given.

II. EXPERIMENTAL METHODS

A crystal of TiO_2 containing 0.01% nickel was used as its own dielectric cavity.¹ The rutile dielectric resonator has the advantage of possessing many resonances with large Q 's. The loaded Q 's (Q_L) were around 15 000 at 77°K and about 50 000 at 4.2°K .

The quality factor of the material (Q_M) can be obtained from measurements of the loaded cavity Q by using the relationship:

$$Q_{LR}^{-1} = Q_{L0}^{-1} + Q_M^{-1},$$

where Q_{LR} and Q_{L0} are the measured cavity Q 's on respectively, off paramagnetic resonance. The magnetic Q is a quality factor representing the absorption losses of the material and is defined by²:

$$Q_M = \frac{h\Delta\nu}{8\pi(n_2 - n_1)|\mu_{21}|^2 F},$$

where $\Delta\nu$ is the paramagnetic linewidth expressed in cycles per second; $(n_2 - n_1)$ is the population difference between the two levels per cc; $|\mu_{21}|$ is the matrix element for the transition and F is the filling factor which is unity for this cavity.

In principle, the concentration, which is simply related to the population difference $(n_2 - n_1)$, can be obtained from a measurement of the magnetic Q . The difficulty arises in trying to calculate the term $|\mu_{21}|$. $|\mu_{21}|$ depends on the orientation of the high-frequency magnetic field and therefore is dependent on the mode of the dielectric resonator which is unknown. Two approximate methods were used to obtain the concentration of the paramagnetic ions.

In one method, Q_M was measured for a large number of cavity resonances. The average of these values was then used in conjunction with the calculated space average value of $|\mu_{21}|$. In the second method, it was assumed that the smallest Q_M value corresponded to the largest value of $|\mu_{21}|$. This value of $|\mu_{21}|$ was computed and substituted in the formula for Q_M . From this the concentration was calculated. Both methods gave values for the concentration which agreed with each other within a factor of two.

In this manner it was found that the nickel-doped rutile crystal contained about eighty parts per million Ni^{2+} , five parts per million Ni^{3+} and two parts per million of a light-generated nickel center.

The microwave spectrometer that was used consisted of a stabilized source and a superheterodyne detection scheme with scope presentation.

The crystal was oriented with x-ray analysis by G. W. Neighbor of RCA Laboratories. The crystallographic axes were independently checked by observing

† Partially supported by the U. S. Army Signal Corps.

* Now at Chalmers University of Technology, Gothenburg, Sweden.

¹ (a) H. J. Gerritsen and H. R. Lewis, *Quantum Electronics* (Columbia Press, New York, 1960), p. 385. (b) A. Okaya, *Proc. IRE* 48, 1921 (1960).

² T. H. Maiman, *Quantum Electronics* (Columbia Press, New York, 1960), p. 324.